

Quantitative measurement of cerebral blood flow in a juvenile porcine model by depth-resolved near-infrared spectroscopy

Jonathan T. Elliott
Mamadou Diop

University of Western Ontario
Department of Medical Biophysics
London, Ontario N6A 3K7 Canada
and
Lawson Health Research Institute
Imaging Program
London, Ontario N6A 4V2 Canada

Kenneth M. Tichauer

Lawson Health Research Institute
Imaging Program
London, Ontario N6A 4V2 Canada

Ting-Yim Lee

University of Western Ontario
Department of Medical Biophysics
London, Ontario N6A 3K7 Canada
and
Lawson Health Research Institute
Imaging Program
London, Ontario N6A 4V2 Canada
and
Robarts Research Institute
Imaging Research Laboratories
London, Ontario N6A 5K8 Canada

Keith St. Lawrence

University of Western Ontario
Department of Medical Biophysics
London, Ontario Canada N6A 3K7 Canada
and
Lawson Health Research Institute
Imaging Program
London, Ontario N6A 4V2 Canada

1 Introduction

Traumatic brain injury (TBI) is the single most common cause of death and disability among children and young adults.¹ Due to the brain's high-energy demands and limited substrate storage, a primary concern during the acute recovery stage following TBI is the avoidance of cerebral ischemia. A variety of complications can impair cerebral blood flow (CBF) during this stage, including systemic hypotension, increased intracranial pressure (ICP), and spontaneous cerebral vessel constriction, all of which independently worsen outcome.² Consequently, monitoring CBF could help guide therapeutic interventions to prevent secondary brain injury caused by these potential complications.^{3,4} Cerebral blood flow can be

Abstract. Nearly half a million children and young adults are affected by traumatic brain injury each year in the United States. Although adequate cerebral blood flow (CBF) is essential to recovery, complications that disrupt blood flow to the brain and exacerbate neurological injury often go undetected because no adequate bedside measure of CBF exists. In this study we validate a depth-resolved, near-infrared spectroscopy (NIRS) technique that provides quantitative CBF measurement despite significant signal contamination from skull and scalp tissue. The respiration rates of eight anesthetized pigs (weight: 16.2 ± 0.5 kg, age: 1 to 2 months old) are modulated to achieve a range of CBF levels. Concomitant CBF measurements are performed with NIRS and CT perfusion. A significant correlation between CBF measurements from the two techniques is demonstrated ($r^2=0.714$, slope=0.92, $p<0.001$), and the bias between the two techniques is $-2.83 \text{ mL} \cdot \text{min}^{-1} \cdot 100 \text{ g}^{-1}$ ($\text{CI}_{0.95}$: $-19.63 \text{ mL} \cdot \text{min}^{-1} \cdot 100 \text{ g}^{-1} - 13.9 \text{ mL} \cdot \text{min}^{-1} \cdot 100 \text{ g}^{-1}$). This study demonstrates that accurate measurements of CBF can be achieved with depth-resolved NIRS despite significant signal contamination from scalp and skull. The ability to measure CBF at the bedside provides a means of detecting, and thereby preventing, secondary ischemia during neurointensive care.
© 2010 Society of Photo-Optical Instrumentation Engineers. [DOI: 10.1117/1.3449579]

Keywords: near-infrared spectroscopy; traumatic brain injury; cerebral blood flow; indocyanine green; depth resolved; Monte Carlo.

Paper 09576RR received Dec. 27, 2009; revised manuscript received Apr. 21, 2010; accepted for publication Apr. 26, 2010; published online Jun. 15, 2010.

measured by a number of imaging techniques such as computed tomography (CT), magnetic resonance imaging (MRI), and positron emission tomography (PET). However, these modalities are of limited use in intensive care, since patients are often unstable and not easily transported to imaging suites. Therefore, a method of measuring CBF that can be employed directly at the bedside is an attractive alternative.

Near-infrared spectroscopy (NIRS) has emerged over the last decade as a promising method for assessing cerebral hemodynamics and oxygenation. Techniques for measuring CBF with NIRS have been developed that employ either a change in arterial oxygenation or a bolus injection of the light absorbing dye indocyanine green (ICG), as a flow tracer. Both methods have been shown to provide accurate CBF measurements in animal models and neonates.⁵⁻¹⁰ However, when applied to juvenile or adult subjects, measuring CBF accurately has

Address all correspondence to: J. T. Elliott, Imaging Program, Lawson Health Research Institute, 268 Grosvenor St., London, Ontario N6A 4V2 Canada. Tel: (519) 646-6000 ext. 64836; Fax: (519) 645-6110; E-mail: jelliott@lawsonimaging.ca

proven difficult. The main reason for this reduced accuracy is the non-negligible effects on the near-infrared signal of the extracerebral layer (ECL) comprised of skin, muscle, and skull. If contamination by the ECL layer is not accounted for, CBF will be underestimated due to the overestimation of the optical pathlength through brain.¹¹⁻¹³ As such, NIRS has yet to develop into a clinically feasible method for patients older than a few weeks of age, and clinicians continue to rely on invasive subdural CBF techniques or intracranial pressure (ICP) probes to infer changes in cerebral hemodynamics. Not only do these techniques carry a risk of infection and bleeding, evidence suggests that adhering to a set ICP threshold does not always ensure adequate oxygen delivery, owing to differences in intracranial compliance between patients.^{14,15}

We present a depth-resolved continuous-wave NIRS approach that is capable of accurately measuring CBF in the presence of significant signal contamination from extracerebral tissue. The approach is based on our previously developed method of measuring CBF in a neonatal porcine model.⁷ Depth sensitivity was improved by collecting NIR signals from two detection probes placed at different distances from the source. The correlation between the depth of light penetration and source-detector distance formed the basis for the separation of intra- and extracerebral signals.¹⁶ Monte Carlo simulations and an *a priori* knowledge of the ECL thickness from CT images were used to quantify the brain optical path length; this was then used to reconstruct the time-concentration curve of ICG in brain, from which CBF was determined. The primary aim of this study was to validate the depth-resolved NIRS technique by collecting measurements of CBF with NIRS and CT perfusion¹⁷ over a range of hemodynamic states in juvenile pigs. More simplistic NIRS methods of measuring CBF were also performed to demonstrate the improved accuracy obtained with the proposed technique.

2 Materials and Methods

2.1 Animal Experiment

The study was approved by the Animal Use Subcommittee of the Canadian Council on Animal Care at the University of Western Ontario. Juvenile Duroc pigs were delivered from a local supplier on the morning of the experiment. Pigs were tracheotomized and mechanically ventilated while anaesthetized by 3% isoflurane. Cannulae were inserted into each ear for injection of the NIRS and CT contrast agents. An additional cannula was inserted into a femoral artery for continuous monitoring of arterial blood pressure and to allow blood samples to be collected for gas and glucose analysis. Following the surgical procedure, isoflurane was reduced to 1.75% and the animals were allowed to stabilize for 1 h before CBF measurements were collected.

Near-infrared spectroscopy and CT measurements of CBF were collected concomitantly over a range of blood flow values. The range was achieved by adjusting the respiratory rate in each animal to produce distinct levels of arterial blood CO₂ tension (PaCO₂): hypocapnia (PaCO₂ < 28 mmHg), normocapnia (PaCO₂ ≈ 40 mmHg), and hypercapnia (PaCO₂ > 50 mmHg).

2.2 Instrumentation

An in-house-developed continuous-wave spectrometer was used to collect broadband, near-infrared intensity data.¹⁸ The main components of the system included an illumination unit, a multiplexer, and a spectrometer consisting of a holographic grating and a cooled charge-coupled device (CCD). The illumination unit was a 50-W quartz, halogen light bulb that was bandpass filtered to remove light outside the 600- to 1000-nm range. The filtered light was coupled to a 2-m fiber optic bundle (emission optode) with a numerical aperture of 0.55 and a 3.5-mm-diam active area. The opposite end of the emission optode was placed on the scalp of the animal and held in position by a specially designed probe holder. Two optical fiber bundles (detection optodes) with the same specifications as the emission optode were positioned at 1- and 3-cm distances from the emitter to collect light that traveled through the multilayered tissue. Light collected by the detection probes was sequentially recorded at intervals of 200 ms using a multiplexer, as described in detail elsewhere.¹⁸

2.3 Near-Infrared Spectroscopic Measurements of Cerebral Blood Flow

Cerebral blood flow was measured using a bolus-tracking method that requires an intravenous bolus injection of ICG (0.1 mg/kg), followed by continuous measurements of the time-varying concentrations of ICG in arterial blood and brain tissue.⁷ The arterial concentration $c_a(t)$ was measured by a dye densitogram (model DDG-2001 A/K, Nihon Kohden, Tokyo, Japan), and the brain tissue concentration $c_{icg}(t)$, was measured by NIRS. The two concentration curves are related by the following equation:

$$c_{icg}(t) = c_a(t) * [CBF \cdot IRF(t)], \quad (1)$$

where $[CBF \cdot IRF(t)]$ is the flow-scaled impulse residue function (IRF), and $*$ represents the convolution operator. A necessary assumption is that blood flow remains constant during the bolus-tracking experiment, which typically lasts about 70 s. An in-house-developed deconvolution routine was used to calculate $CBF \cdot IRF(t)$ from the measured arterial and tissue concentration curves.¹⁷

2.4 Single-Probe Near-Infrared Spectroscopy

If it is assumed that the head is a homogeneous medium, i.e., the contribution from the ECL is negligible, then the modified Beer-Lambert law can be used to determine time-dependent changes in the concentrations of chromophores in brain from the change in light attenuation $\Delta A(\lambda, t)$ measured from a single detector:

$$\Delta A(\lambda, t) = \sum_i \varepsilon_i(\lambda) \cdot \Delta c_i(t) \cdot DPL. \quad (2)$$

In this equation, λ represents wavelength, $\varepsilon_i(\lambda)$ is the wavelength-dependent extinction coefficient of each chromophore (corrected for the wavelength dependence of the path length¹⁹), $\Delta c_i(t)$ is the concentration change in the i 'th chromophore, and DPL is the total differential pathlength in the medium, averaged across the fitting range 800 to 880 nm. Without attempting to remove ECL signal contamination, the

absolute change in the tissue concentration of ICG $\Delta c_{\text{icg}}(t)$ following an injection of the dye can be determined from $\Delta A(\lambda, t)$ data acquired at a source-detection distance of 3 cm. By collecting broadband NIRS spectra, the DPL can be determined by second differential analysis using the spectral features of water absorption, which are distinct at 740 and 830 nm, and assuming a water concentration in the brain of 80%.²⁰ This single-probe (SP) homogenous approach is referred to as SP-NIRS.

2.5 Depth-Resolved Near-Infrared Spectroscopy

If the ECL is non-negligible, brain signal can potentially be resolved with NIRS by modeling the head as a two-layered medium and simultaneously collecting ICG tissue concentration curves from two detection optodes placed at different source-detector distances. The modified Beer-Lambert law can be generalized for this collection geometry as follows:²¹

$$A(\lambda, t) = \sum_i \sum_j \varepsilon_i(\lambda) \cdot c_{i,j}(t) \cdot \text{MPP}_j + G(\lambda), \quad (3)$$

where $A(\lambda)$ is the wavelength-dependent attenuation measured by the detector, $c_{i,j}$ is the concentration of the i 'th chromophore in the j 'th layer, MPP_j is the mean partial path length of light in the j 'th layer, and $G(\lambda)$ is the loss of light from scattering. For a two-layered medium, a change in attenuation measured by detector probe p can be expressed as

$$\begin{aligned} \Delta A_p(\lambda, t) = & \sum_i \varepsilon_i(\lambda) \cdot \Delta c_{i,\text{ECL}}(t) \cdot \text{MPP}_{p,\text{ECL}} \\ & + \sum_i \varepsilon_i(\lambda) \cdot \Delta c_{i,\text{brain}}(t) \cdot \text{MPP}_{p,\text{brain}}. \end{aligned} \quad (4)$$

Assuming all other chromophore concentrations remain constant, the change in the ICG concentration in brain following bolus injection is given by:

$$\Delta c_{\text{icg,brain}}(t) = \frac{\Delta A_2(\lambda, t) - r \cdot \Delta A_1(\lambda, t)}{\varepsilon_{\text{icg}}(\lambda) \cdot (\text{MPP}_{2,\text{brain}} - r \cdot \text{MPP}_{1,\text{brain}})}, \quad (5)$$

where the subscripts 1 and 2 refer to source-detector distances of 1 and 3 cm, respectively, and $r = (\text{MPP}_{2,\text{ECL}} / \text{MPP}_{1,\text{ECL}})$.

To determine $\Delta c_{\text{icg,brain}}(t)$ from Eq. (5), the mean partial path lengths must be estimated. This was done in a multistep process using a library of potential MPPs derived from Monte Carlo simulations generated for various ECL thicknesses and various ECL component (skull, scalp, and CSF) ratios (see Sec. 2.7). The first step was to acquire an anatomical image of the subject's head to determine the thickness of the ECL. Second, a set of potential MPPs was selected from the library from simulations that employed ECL thicknesses within 20% of the measured value. Third, for each potential set of MPPs, second derivative spectroscopy was applied to baseline attenuation data (i.e., prior to ICG injection) to calculate the concentration of water in the brain. Finally, the set of MPP values that resulted in a water concentration closest to the assumed value of 80% was chosen and used in Eq. (5), with $\Delta A(\lambda, t)$ data from 800 to 880 nm to calculate $\Delta c_{\text{icg,brain}}(t)$. Once the ICG concentration curve for brain tissue was ex-

Table 1 Optical properties used in the Monte Carlo simulations to calculate mean partial pathlengths.⁴⁰

Medium	μ'_s (cm ⁻¹)		μ_a (cm ⁻¹)	
	760 nm	830 nm	760 nm	830 nm
Scalp	7.3	6.6	0.177	0.191
Skull	9.3	8.6	0.125	0.136
CSF	0.1	0.1	0.021	0.026
Brain	11.8	11.1	0.195	0.106

tracted from the multiprobe data, CBF was determined from Eq. (1). We refer to this depth-resolved (DR) approach as DR-NIRS.

2.6 Simple-Subtraction Technique

If anatomical information is not made available to characterize the ECL, it has been proposed that ECL contamination be reduced by calculating the difference in attenuation measurements from the two optodes.²² If the light collected by the optode placed at 1 cm is assumed to have interrogated only the ECL, and the path length of light through the ECL is assumed to be the same for light collected at both distances (i.e., $r=1$), Eq. (5) reduces to

$$\Delta c_{\text{icg,brain}}(t) = \frac{\Delta A_2(\lambda, t) - \Delta A_1(\lambda, t)}{\varepsilon_{\text{icg}}(\lambda) \cdot \text{MPP}_{2,\text{brain}}}. \quad (6)$$

The brain optical path length $\text{MPP}_{2,\text{brain}}$ can then be estimated from the DPL and an assumed fractional brain contribution.¹¹ Since the DPL cannot be measured accurately by broadband NIRS due to tissue heterogeneity, a pathlength factor of 5.9 was chosen²³ and the fraction of the DPL through the brain was assumed to be 35%. This value was chosen from the Monte Carlo simulations presented in the following section. The same value of $\text{MPP}_{2,\text{brain}}$ was used to analyze all datasets. This simple subtraction technique is referred to as SS-NIRS.

2.7 Monte Carlo Library Generation

Monte Carlo simulations have been extensively used to model light propagation in multilayered media.²¹ To generate the MPPs required for Eqs. (3)–(5), we developed a Monte Carlo code in C++ using the optical properties listed in Table 1 and based on the algorithm described by Wang, Jacques, and Zheng.²⁴ A library of MPP values was generated for combinations of different ECL thicknesses (5 to 20 mm in steps of 1 mm) and relative scalp-to-bone ratios (3:7, 4:6, 5:5, 6:4, and 7:3) at two wavelengths (760 and 830 nm). The use of only two wavelengths to characterize MPP over the fitting range was necessary, because Monte Carlo simulations are time consuming. These particular wavelengths were used because their optical properties for the various extra- and intracerebral tissues are well documented, and they are also close to a distinct water feature at 740 nm and the peak absorption of

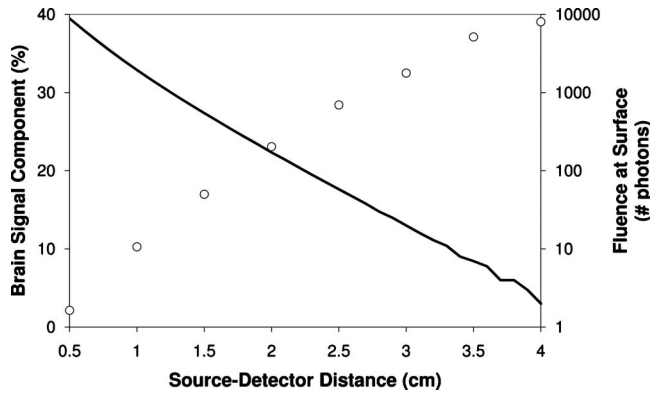


Fig. 1 Relative brain signal component (open circles) as a function of source-detector distance for Monte Carlo simulations performed using the optical properties in Table 1 and assuming an ECL thickness of 10 mm. The corresponding fluence at the surface of the head for 10^8 simulated photons is shown on the right axis (solid line), illustrating the tradeoff between penetration depth and signal intensity.

ICG at 805 nm. Small discrepancies between wavelengths were accounted for by correcting $\varepsilon(\lambda)$ for the wavelength dependency of path length.¹⁹

Monte Carlo simulations were also used to determine the optimal source-detector distance for the experiments. The relative contribution of the brain to the total optical path length, defined as the ratio between the MPP in the brain layer and the total DPL, was calculated at different source-detector distances using the optical properties described in Table 1 for an ECL thickness of 10 mm. The predicted contribution is displayed in Fig. 1, along with the relative fluence of photons at the scalp surface. Based on these simulations, source-detector distances of 1 and 3 cm were chosen, as signals collected at these distances differed sufficiently in terms of their sensitivity to the two layers and provided fluence rates acceptable for signal-to-noise considerations. Simulations were performed on the Shared Hierarchical Academic Research Computing Network (SHARCNET) system (University of Western Ontario, Canada), a high performance computer cluster, and required 4 to 6 CPU hours per simulation on average for 10^8 photons on a 2.2-GHz CPU core.

2.8 Computed Tomography Perfusion Imaging

Computed tomography images of CBF were acquired using a LightSpeed QXi multislice CT scanner (GE Healthcare, Milwaukee, Wisconsin). Eight 5-mm-thick coronal slice scans (80 kVp, 190 mA) were collected at 1-s intervals for 40 s upon injection of 1.0 mL/kg of the iodinated contrast agent iohexol (300 mg I/mL; Omnipaque™, GE Healthcare, Waukesha, Wisconsin); the injection rate was 1 ml/s. Parametric maps of CBF were generated from the cine images using CT PERFUSION 3 software (GE Healthcare). Regions of interest were defined on the CBF images that corresponded to the brain volume interrogated by the NIRS probes [Fig. 2(a)]. The thickness of the ECL was measured using anatomical CT images acquired at the start of the experiment. Since the probe holder was visible on the CT image, ECL thickness could be measured directly below the location of the optodes [Fig. 2(b)].

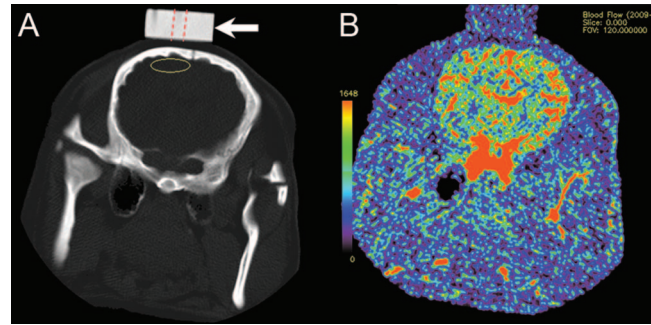


Fig. 2 (a) Computed tomography anatomical image showing the region of interest (yellow outline) directly below the optical probe holder (white arrow). Red dashed lines on the probe holder indicate position of the optode. (b) Corresponding cerebral blood flow map determined by CT perfusion.

2.9 Statistical Analysis

All data are presented as mean \pm SE unless otherwise stated. SPSS 16.0 (SPSS, Chicago, Illinois) was used for all statistical analyses, and statistical significance was defined as $p < 0.05$. Physiological parameters were analyzed using one-way analysis of variances (ANOVAs) and a Tukey's honestly significant difference (HSD) test for *post hoc* analyses. Correlations between CT and NIRS CBF were analyzed using parametric linear regression. Nonparametric analysis was used to analyze the relationship between the errors in the NIRS-CBF measurements and ECL thickness.

3 Results

Cerebral blood flow measurements were acquired in eight juvenile pigs. All pigs were between one and two months of age with a mean weight of 16.2 ± 0.5 kg. The thickness of the ECL, as determined from anatomical CT images, ranged from 7.5 to 14.5 mm, with a mean value of 10.4 ± 0.6 mm. In total, 25 ICG runs were completed; however, four NIRS measurements could not be analyzed. In three cases, the concentration of ICG injected was below the threshold required for accurate DDG analysis, and in one case the CT contrast agent concentration was too low. The results of the physiological parameters for the eight pigs at the three different conditions are summarized in Table 2. As expected, average PaCO₂ and pH values were significantly different between hypo-, normo-, and hypercapnia groups ($p < 0.05$). No statistically significant differences were observed for any of the other physiological parameters.

To determine the error caused by ignoring the ECL, the SP-NIRS approach was applied to ICG tissue concentration curves acquired with a source-detection distance of 3 cm, and the resulting CBF estimates were compared with CBF measured by CT perfusion. Figure 3(a) depicts an example of the time-dependent change in optical density measured at both optode distances following ICG injection. Figure 4 shows the SP-NIRS CBF measurements plotted as a function of the corresponding CBF measurements acquired with CT perfusion. The SP-NIRS technique consistently underestimated CBF, and no significant correlation was observed between CBF measurements from the two techniques. The mean CBF determined by SP-NIRS was 18.17 ± 3.26 mL \cdot min⁻¹ \cdot 100 g⁻¹,

Table 2 Physiological parameters during hypocapnia, normocapnia, and hypercapnia. Values are mean \pm SE. * $p < 0.05$ compared with hypocapnia. † $p < 0.05$ compared with normocapnia. †† n_x refers to the number of ICG runs acquired at each capnic level.

	Hypocapnia ($n_x=6$)††	Normocapnia ($n_x=13$)	Hypercapnia ($n_x=6$)
Heart rate, beats/min	122 \pm 5	132 \pm 5	159 \pm 15*
Mean arterial pressure, mmHg (kPa)	54.5 \pm 2.0 (7.3 \pm 0.3)	57.8 \pm 1.9 (7.7 \pm 0.2)	63.2 \pm 1.9* (8.4 \pm 0.2)
Arterial PCO ₂ , mmHg (kPa)	22.6 \pm 1.3 (3.0 \pm 0.2)	38.9 \pm 1.2* (5.2 \pm 0.1)	57.4 \pm 4.4*† (7.6 \pm 0.6)
Arterial PO ₂ , mmHg (kPa)	238.7 \pm 21.0 (31.8 \pm 2.8)	227.1 \pm 15.8 (30.3 \pm 2.1)	212.9 \pm 22.1 (28.4 \pm 2.9)
Arterial pH	7.58 \pm 0.02	7.43 \pm 0.01*	7.30 \pm 0.03*†

which was significantly different from the mean CBF value determined by CT perfusion ($69.91 \pm 3.25 \text{ mL} \cdot \text{min}^{-1} \cdot 100 \text{ g}^{-1}$, $p < 0.001$).

Figure 5 shows CBF values derived from the SS-NIRS technique plotted as a function of the corresponding CBF values determined from CT perfusion. Similar to the SP-NIRS results, no significant correlation was observed between CBF measurements from the two techniques. The mean CBF calculated by SS-NIRS ($42.80 \pm 7.58 \text{ mL} \cdot \text{min}^{-1} \cdot 100 \text{ g}^{-1}$) was greater than that determined using SP-NIRS, but still under-

estimated the mean CBF calculated from the CT perfusion dataset.

The correlation between CBF measurements from DR-NIRS and CT perfusion is shown in Fig. 6. In this case, a strong, statistically significant correlation was revealed ($r^2=0.714$, slope=0.92, $p < 0.001$). The mean CBF measured using the DR-NIRS approach was $64.93 \pm 3.47 \text{ mL} \cdot \text{min}^{-1} \cdot 100 \text{ g}^{-1}$, which was not significantly different from that measured by CT perfusion. A Bland-Altman plot was used to investigate the existence of any bias in the CBF measurements, and to determine the variability in the measurements (Fig. 7). The mean difference between the two techniques was $-2.83 \text{ mL} \cdot \text{min}^{-1} \cdot 100 \text{ g}^{-1}$. The limits of agreement, i.e., the region in which 95% of the differences exist, were -19.63 and $14.00 \text{ mL} \cdot \text{min}^{-1} \cdot 100 \text{ g}^{-1}$. No discernible CBF-dependent errors were observed.

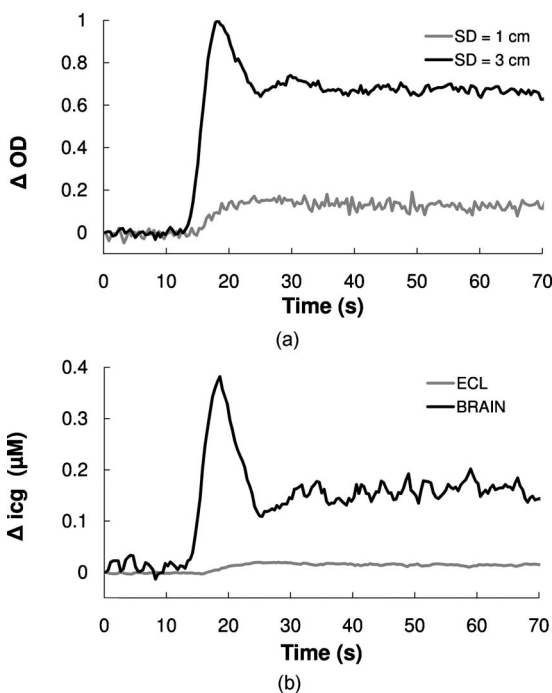


Fig. 3 (a) Change in optical density following ICG injection at 1- and 3-cm detector probes, and (b) the corresponding change in ICG concentration in the ECL and brain following data processing by the DR-NIRS method. Data are from the same ICG run in an animal with an ECL thickness of 14 mm.

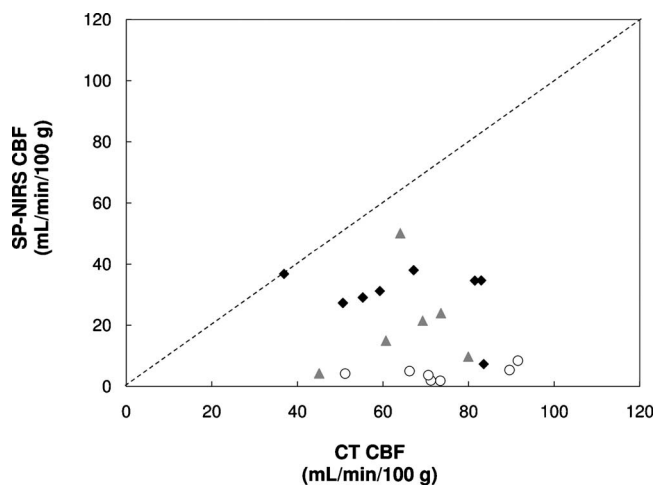


Fig. 4 Correlation plot comparing CBF measurements acquired by CT perfusion and single-probe NIRS. Symbols represent the data grouped according to ECL thickness: less than or equal to 8 mm (solid diamonds), between 8 and 12 mm (shaded triangles), and greater than or equal to 12 mm (open circles). No significant correlation between the CBF measurements from the two techniques was detected. The line of unity (dashed line) is shown for comparison.

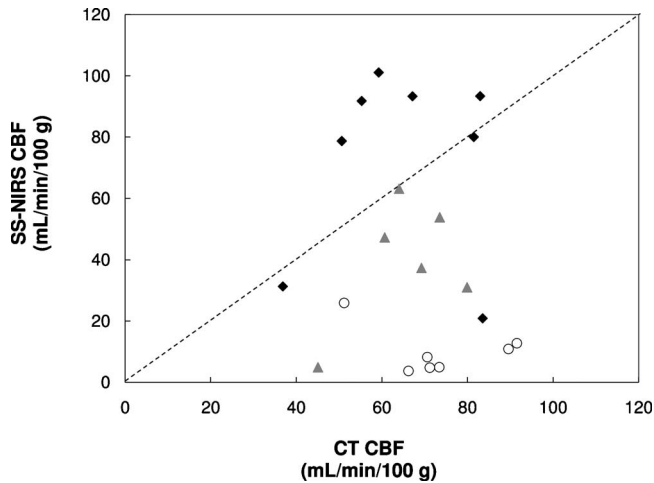


Fig. 5 Correlation plot comparing the CT and SS-NIRS measurements of CBF. Symbols represent three ECL groups described in Fig. 4. No significant correlation between the two measurements was detected. The dashed line indicates the line of unity.

Nonparametric regression analysis was performed to further investigate the relationship between ECL thickness and the percent difference between CT perfusion and CBF values obtained with each of the NIRS techniques. Significant correlations were observed for both SP-NIRS ($\rho = -0.884$, $p < 0.001$) and SS-NIRS ($\rho = -0.861$, $p < 0.001$). In contrast, there was no correlation between ECL thickness and percent difference in CBF values for DR-NIRS.

4 Discussion

An integral part of critical care management of traumatic brain injury patients is the maintenance of adequate CBF to avoid secondary brain injury. Near-infrared spectroscopy has long been recognized for its potential as a noninvasive bedside cerebral monitor due to its portability and sensitivity to

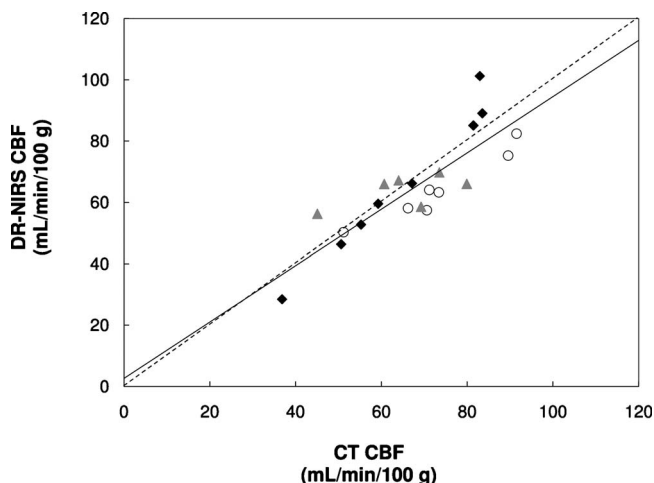


Fig. 6 Correlation plot comparing the CT and DR-NIRS measurements of CBF. Symbols represent three ECL groups described in Fig. 4. The solid line represents the line of regression ($r^2 = 0.714$, slope = 0.92, intercept = 2.7, $p < 0.001$), and the line of unity (dashed line) is shown for comparison.

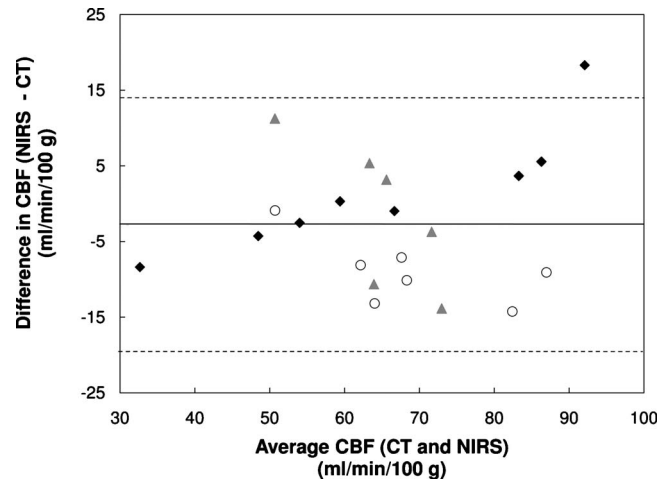


Fig. 7 Bland-Altman plot comparing CT and DR-NIRS measurements of CBF. Symbols represent three ECL groups, as described in Fig. 4. The mean difference between the two measurements (solid line) is $-2.83 \text{ mL} \cdot \text{min}^{-1} \cdot 100 \text{ g}^{-1}$. The limits of agreement (dashed lines), within which 95% of the differences reside, are 13.97 and $-19.63 \text{ mL} \cdot \text{min}^{-1} \cdot 100 \text{ g}^{-1}$.

cerebral hemodynamics.²⁵ However, its application to adult patients has been challenged by the significant signal contamination from the scalp and skull. Previous studies have reported that CBF collected using traditional NIRS approaches can be underestimated by more than a factor of 3, due primarily to the increase in optical path length through extracerebral tissue.¹¹ Moreover, not only does ECL contamination affect the accuracy of the CBF measurements, studies using ICG bolus tracking methods have found that NIRS is also insensitive to changes in CBF, which questions if NIRS can even be used to monitor relative CBF.^{22,26} To overcome this major hurdle, we proposed a novel depth-resolved NIRS approach that uses Monte Carlo simulations in conjunction with the two-layer modified Beer-Lambert law to extract the cerebral ICG concentration curve from multidistance NIRS data. The use of subject-individualized Monte Carlo simulations to model depth-resolved NIRS is a logical extension of previous work using a similar technique to measure changes in brain oxygenation during neural activation.²⁷ Selection of the appropriate simulation parameters for each animal was based on its specific ECL geometry (i.e., thickness and relative scalp-to-skull ratio) determined from anatomical CT images. A fixed cerebral water concentration provided an additional constraint in the selection process. The main finding of this work was that CBF measurements obtained with our Monte Carlo driven, depth-resolved NIRS technique correlated well with CT perfusion data (a clinically validated and widely used technique for measuring CBF in humans.^{28,29}) As a corollary, we found that the more simplistic SP-NIRS and SS-NIRS techniques did not provide reliable measurements of CBF.

It was expected from previous studies^{11,12} that the SP-NIRS technique would be inadequate for measuring CBF in the intact adult head, since the cerebral NIR signal comprises only about 30% of the total signal at a source-detector distance of 3 cm (see Fig. 1). Qualitatively, this effect can be seen in the ICG data, an example of which is shown in Fig. 3(a). Signal collected by the 3-cm detector probe demon-

strates a relatively slow washout, typical of ECL tissue, attributable to its low blood flow. The effect of the significant extracerebral optical path length was evident by the large underestimations of CBF, calculated from the long-distance NIRS data compared to the measurements acquired with CT perfusion. Furthermore, no correlation between the two techniques was observed over a range of CBF from 35 to 90 $\text{ml} \cdot \text{min}^{-1} \cdot 100 \text{ g}^{-1}$. These results agree with previous studies conducted in humans,^{12,13} and clearly demonstrate that SP-NIRS is unsuitable for measuring CBF in adults.

Marginal improvements were observed for SS-NIRS, which relied on an assumed value of the mean partial path length in brain, over the SP-NIRS approach; however, it also performed poorly relative to DR-NIRS. It might be anticipated that even if SS-NIRS cannot accurately measure absolute CBF, a correlation with CT perfusion could be expected, but this was not observed. The most likely explanation for this discrepancy is that the relative contributions of brain and ECL varied substantially from experiment to experiment, as suggested by the dependency of SS-NIRS error on the ECL thickness revealed by the nonparametric analysis. Further analysis of the data revealed that the error in the assumed “*r*-ratio” was correlated with the error in SS-NIRS measurement of CBF ($r = -0.76$, $p < 0.01$), suggesting that the large variability in the SS-NIRS data has its source in the error of MPP values used in this approach. Since the calculation of CBF is heavily dependent on the height of the ICG curve, which in turn is dependent on the chosen value of brain MPP, any discrepancy between the assumed MPP and the true value will lead to considerable variance in the CBF estimate. These findings suggest that to measure CBF precisely, a case-by-case method of calculating the MPP values is a prerequisite. These results also provide a plausible reason for the failure of SS-NIRS to detect changes in CBF in healthy human subjects, as reported in a recent study,²² and may help to explain some of the contamination issues observed in studies measuring cerebral blood saturation by spatially resolved NIRS.³⁰

The approach presented in the current study is based on our previously validated technique using broadband continuous-wave NIRS.⁷ In contrast to the simpler techniques presented before, the DR-NIRS technique attempted to correct for the primary sources of intersubject variability. By using independent Monte Carlo simulations with *priori* information of the ECL thickness, MPP values can be defined on a subject-by-subject basis. Furthermore, by using a continuous-wave, broadband NIRS system, second derivative spectroscopy can assist with selecting the appropriate MPP values. By virtue of the fact that the water concentration in brain is known (80%) and relatively stable,²⁰ the MPP selection process was constrained to only those choices that met this criterion. Finally, our system uses a shutter multiplexing system that allows for rapid collection of NIR signals from multiple probes with high fidelity.¹⁸ It is likely that these characteristics contributed to the strong correlation that was observed between CBF measurements from CT perfusion and DR-NIRS (Fig. 6), and also resulted in the small bias revealed by the Bland-Altman method (Fig. 7). When compared with the previous validation study published by our group for the neonatal pig model, which also used CT perfusion,⁷ the 95% confidence intervals shown in the Bland-Altman plot were only slightly larger ($\pm 16.8 \text{ mL} \cdot \text{min}^{-1} \cdot 100 \text{ g}^{-1}$ compared to

$\pm 12.7 \text{ mL} \cdot \text{min}^{-1} \cdot 100 \text{ g}^{-1}$ in the previous study). Given the sources of uncertainty introduced by the depth-resolved approach, as well as the decreased signal-to-contrast ratio, it is encouraging to note that the difference in precision was only marginal.

From the time when the possibility of using multidistance NIRS to separate intra- and extracerebral ICG concentration curves was first demonstrated by Hongo et al.,¹⁶ several other groups have also incorporated ICG bolus tracking methods with other depth-resolved NIRS techniques. Liebert and associates have employed time-resolved NIRS to isolate the cerebral ICG concentration curve in a number of studies,³¹⁻³³ and using the variance of the time-of-flight data to enhance depth sensitivity, they demonstrated that NIRS could detect cerebral ischemia in a stroke patient.³² Frequency-domain analysis has also been used to discriminate between intra- and extracerebral ICG concentration curves using the intrinsic sensitivity of the modulation phase to light absorption in deeper tissue.^{34,35} However, none of these studies attempted to quantify CBF, which requires measuring the absolute ICG concentration in brain. Functional NIRS studies involving task activation have approached the problem of scalp contamination by exploiting two properties: first, activation causes regional changes in blood flow, whereas scalp interference is global; and second, scalp signal interference contains a significant portion that is uncorrelated with CBF.³⁶⁻³⁸ Neither of these assumptions would be valid in the present study, since blood flow responses to capnic changes could occur in the scalp as well as the brain, and the brain and ECL ICG traces are strongly correlated.

There are some limitations/concerns with our DR-NIRS approach that need to be addressed prior to clinical implementation. The first concern pertains to the reliance on *priori* knowledge of the ECL geometry from anatomical imaging. Certainly, a completely independent technique would be more attractive and may potentially emerge in the future. However, given that standard procedure for head trauma neurological assessment on admittance includes CT or MRI scanning, the requirement of this additional information for subsequent NIRS measurements does not represent a significant burden. A second concern is the possibility that the two-layer Beer-Lambert model used to characterize light propagation through the pig head may not adequately represent the human head. However, a similar model has been used to detect changes in cerebral oxygenation in human subjects.³⁹ Our approach also relied on assumed optical properties for the ECL. While the selected brain MPP value was constrained by the known water concentration, further work is required to determine how uncertainties in the assumed scattering and absorption coefficients for the different extracerebral layers (scalp, skull, and CSF) affect the accuracy of the CBF measurements. Because MPPs were calculated at a single wavelength, representative of the mean MPP within the fitting range, we performed further analysis to determine the potential error in CBF measurement caused by this process. We compared CBF values obtained using the MPP calculated at 830 nm with CBF determined using MPP values defined at each wavelength between 800 and 880 nm. The error between the measurements was less than one percent. Additionally, this study used CT perfusion to validate the blood flow. This process required selecting ROIs underneath the NIRS probe that corresponded

to the area interrogated by the NIR light. To determine the variability in the CBF measurements caused by the variable ROI selection, CBF was measured in three additional ROIs placed 1 cm to the right, to the left, and posterior in two animals. No significant ROI-dependent differences in CBF were detected. A final concern with this study is that the mean thickness of the ECL was 10 mm, and consequently, was more representative of a juvenile patient group than an adult one. Although the results from the animals with an ECL >12 mm were encouraging, more experiments are required to assess our technique with larger ECL thicknesses.

5 Conclusion

The salient finding of the present study is that, in contrast to SP- and SS-NIRS methods, the DR-NIRS technique demonstrates for the first time that accurate measurements of CBF can be acquired with NIRS despite the presence of a significant ECL. These results highlight the promise of using NIRS for acquiring bedside measurements of CBF in neurological intensive care patients, demonstrating the potential of NIRS to greatly improve clinical management of these individuals.

Acknowledgments

This study was supported through grants from the Lawson Health Research Institute and the Heart and Stroke Foundation of Canada. This work was made possible by the facilities of the Shared Hierarchical Academic Research Computing Network (SHARCNET, see <http://www.sharcnet.ca>) and Compute/Calcul Canada. The authors would also like to thank Jennifer Hadway and Lise Desjardins for their help in conducting the animal experiments, and Chris d'Esterre for his assistance in the CT perfusion measurements.

References

1. J. Langlois, Ed., "Traumatic Brain Injury in the United States: Assessing Outcomes in Children, National Center for Injury Prevention and Control of the Centers for Disease Control and Prevention, Atlanta, GA (2000).
2. O. Chaiwat, D. Sharma, Y. Udomphorn, W. M. Armstead, and M. S. Vavilala, "Cerebral hemodynamic predictors of poor 6-month Glasgow Outcome Score in severe pediatric traumatic brain injury," *J. Neurotrauma* **26**(5), 657–663 (2009).
3. S. C. Singhi and L. Tiwari, "Management of intracranial hypertension," *Indian J. Pediatr.* **76**(5), 519–529 (2009).
4. J. P. Jantzen, "Prevention and treatment of intracranial hypertension," *Best Pract. Res. Clin. Anaesthesiol.* **21**(4), 517–538 (2007).
5. G. Themelis, H. D'Arceuil, S. G. Diamond, S. Thaker, T. J. Huppert, D. A. Boas, and M. A. Franceschini, "Near-infrared spectroscopy measurement of the pulsatile component of cerebral blood flow and volume from arterial oscillations," *J. Biomed. Opt.* **12**(1), 014033 (2007).
6. I. Tachtsidis, M. M. Tisdall, T. S. Leung, C. Pritchard, C. E. Cooper, M. Smith, and C. E. Elwell, "Relationship between brain tissue haemodynamics, oxygenation and metabolism in the healthy human adult brain during hyperoxia and hypercapnea," *Adv. Exp. Med. Biol.* **645**, 315–320 (2009).
7. D. W. Brown, P. A. Picot, J. G. Nacini, R. Springett, D. T. Delpy, and T. Y. Lee, "Quantitative near infrared spectroscopy measurement of cerebral hemodynamics in newborn piglets," *Pediatr. Res.* **51**(5), 564–570 (2002).
8. K. M. Tichauer, J. A. Hadway, T. Y. Lee, and K. St. Lawrence, "Measurement of cerebral oxidative metabolism with near-infrared spectroscopy: a validation study," *J. Cereb. Blood Flow Metab.* **26**(5), 722–730 (2006).
9. R. Springett, Y. Sakata, and D. T. Delpy, "Precise measurement of cerebral blood flow in newborn piglets from the bolus passage of indocyanine green," *Phys. Med. Biol.* **46**(8), 2209–2225 (2001).
10. J. Patel, K. Marks, I. Roberts, D. Azzopardi, and A. D. Edwards, "Measurement of cerebral blood flow in newborn infants using near infrared spectroscopy with indocyanine green," *Pediatr. Res.* **43**(1), 34–39 (1998).
11. H. Owen-Reece, C. E. Elwell, W. Harkness, J. Goldstone, D. T. Delpy, J. S. Wyatt, and M. Smith, "Use of near infrared spectroscopy to estimate cerebral blood flow in conscious and anaesthetized adult subjects," *Br. J. Anaesth.* **76**(1), 43–48 (1996).
12. F. Gora, S. Shinde, C. E. Elwell, J. C. Goldstone, M. Cope, D. T. Delpy, and M. Smith, "Noninvasive measurement of cerebral blood flow in adults using near-infrared spectroscopy and indocyanine green: a pilot study," *J. Neurosurg. Anesthesiol.* **14**(3), 218–222 (2002).
13. R. D. Rothoerl, K. M. Schebesch, R. Faltermeier, C. Woertgen, and A. Brawanski, "Lack of correlation between Xenon133 and near infrared spectroscopy/indocyanine green rCBF measurements," *Neurol. Res.* **25**(5), 528–532 (2003).
14. W. L. Wright, "Multimodal monitoring in the ICU: when could it be useful?," *J. Neurol. Sci.* **261**(1–2), 10–15 (2007).
15. M. F. Stiefel, J. D. Udoetuk, A. M. Spiotta, V. H. Gracias, A. Goldberg, E. Maloney-Wilensky, S. Bloom, and P. D. Le Roux, "Conventional neurocritical care and cerebral oxygenation after traumatic brain injury," *J. Neurosurg.* **105**(4), 568–575 (2006).
16. K. Hongo, S. Kobayashi, H. Okudera, M. Hokama, and F. Nakagawa, "Noninvasive cerebral optical spectroscopy: depth-resolved measurements of cerebral haemodynamics using indocyanine green," *Neurol. Res.* **17**(2), 89–93 (1995).
17. A. Cenic, D. G. Nabavi, R. A. Craen, A. W. Gelb, and T. Y. Lee, "Dynamic CT measurement of cerebral blood flow: a validation study," *AJNR Am. J. Neuroradiol.* **20**(1), 63–73 (1999).
18. M. Diop, J. T. Elliott, K. M. Tichauer, T. Y. Lee, and K. St Lawrence, "A broadband continuous-wave multichannel near-infrared system for measuring regional cerebral blood flow and oxygen consumption in newborn piglets," *Rev. Sci. Instrum.* **80**(5), 054302 (2009).
19. M. Cope, "The application of near infrared spectroscopy to non invasive monitoring of cerebral oxygenation in the newborn infant," PhD Thesis, p. 290, Univ. College London, United Kingdom (1991).
20. S. J. Matcher, M. Cope, and D. T. Delpy, "Use of the water absorption spectrum to quantify tissue chromophore concentration changes in near-infrared spectroscopy," *Phys. Med. Biol.* **39**(1), 177–196 (1994).
21. M. Hiraoka, M. Firbank, M. Essenpreis, M. Cope, S. R. Arridge, P. van der Zee, and D. T. Delpy, "A Monte Carlo investigation of optical pathlength in inhomogeneous tissue and its application to near-infrared spectroscopy," *Phys. Med. Biol.* **38**(12), 1859–1876 (1993).
22. H. W. Schyetz, T. Wienecke, L. T. Jensen, J. Selb, D. A. Boas, and M. Ashina, "Changes in cerebral blood flow after acetazolamide: an experimental study comparing near-infrared spectroscopy and SPECT," *Eur. J. Neurol.* **16**(4), 461–467 (2009).
23. P. van der Zee, M. Cope, S. R. Arridge, M. Essenpreis, L. A. Potter, A. D. Edwards, J. S. Wyatt, D. C. McCormick, S. C. Roth, E. O. Reynolds, and D. T. Delpy, "Experimentally measured optical pathlengths for the adult head, calf and forearm and the head of the newborn infant as a function of inter optode spacing," *Adv. Exp. Med. Biol.* **316**, 143–153 (1992).
24. L. Wang, S. L. Jacques, and L. Zheng, "MCML—Monte Carlo modeling of light transport in multi-layered tissues," *Comput. Methods Programs Biomed.* **47**(2), 131–146 (1995).
25. P. W. McCormick, M. Stewart, M. G. Goetting, M. Dujovny, G. Lewis, and J. I. Ausman, "Noninvasive cerebral optical spectroscopy for monitoring cerebral oxygen delivery and hemodynamics," *Crit. Care Med.* **19**(1), 89–97 (1991).
26. T. S. Leung, I. Tachtsidis, M. Tisdall, M. Smith, D. T. Delpy, and C. E. Elwell, "Theoretical investigation of measuring cerebral blood flow in the adult human head using bolus Indocyanine Green injection and near-infrared spectroscopy," *Appl. Opt.* **46**(10), 1604–1614 (2007).
27. T. Yamada, S. Umeyama, and K. Matsuda, "Multidistance probe arrangement to eliminate artifacts in functional near-infrared spectroscopy," *J. Biomed. Opt.* **14**(6), 064034 (2009).
28. A. A. Konstas, G. V. Goldmakher, T. Y. Lee, and M. H. Lev, "Theoretic basis and technical implementations of CT perfusion in acute ischemic stroke, part 2: technical implementations," *AJNR Am. J. Neuroradiol.* **30**(5), 885–892 (2009).

29. A. A. Konstas, G. V. Goldmakher, T. Y. Lee, and M. H. Lev, "Theoretic basis and technical implementations of CT perfusion in acute ischemic stroke, part 1: theoretic basis," *AJNR Am. J. Neuroradiol.* **30**(4), 662–668 (2009).
30. S. Muehlschlegel and E. B. Lobato, "Con: all cardiac surgical patients should not have intraoperative cerebral oxygenation monitoring," *J. Cardiothorac Vasc. Anesth.* **20**(4), 613–615 (2006).
31. A. Liebert, H. Wabnitz, H. Obrig, R. Erdmann, M. Moller, R. Macdonald, H. Rinneberg, A. Villringer, and J. Steinbrink, "Non-invasive detection of fluorescence from exogenous chromophores in the adult human brain," *Neuroimage* **31**(2), 600–608 (2006).
32. A. Liebert, H. Wabnitz, J. Steinbrink, M. Moller, R. Macdonald, H. Rinneberg, A. Villringer, and H. Obrig, "Bed-side assessment of cerebral perfusion in stroke patients based on optical monitoring of a dye bolus by time-resolved diffuse reflectance," *Neuroimage* **24**(2), 426–435 (2005).
33. A. Liebert, H. Wabnitz, J. Steinbrink, H. Obrig, M. Moller, R. Macdonald, A. Villringer, and H. Rinneberg, "Time-resolved multidistance near-infrared spectroscopy of the adult head: intracerebral and extracerebral absorption changes from moments of distribution of times of flight of photons," *Appl. Opt.* **43**(15), 3037–3047 (2004).
34. M. Kohl-Bareis, H. Obrig, J. Steinbrink, J. Malak, K. Uludag, and A. Villringer, "Noninvasive monitoring of cerebral blood flow by a dye bolus method: separation of brain from skin and skull signals," *J. Biomed. Opt.* **7**(3), 464–470 (2002).
35. J. Steinbrink, H. Wabnitz, H. Obrig, A. Villringer, and H. Rinneberg, "Determining changes in NIR absorption using a layered model of the human head," *Phys. Med. Biol.* **46**(3), 879–896 (2001).
36. Q. Zhang, G. E. Strangman, and G. Ganis, "Adaptive filtering to reduce global interference in non-invasive NIRS measures of brain activation: how well and when does it work?," *Neuroimage* **45**(3), 788–794 (2009).
37. S. Kohno, I. Miyai, A. Seiyama, I. Oda, A. Ishikawa, S. Tsuneishi, T. Amita, and K. Shimizu, "Removal of the skin blood flow artifact in functional near-infrared spectroscopic imaging data through independent component analysis," *J. Biomed. Opt.* **12**(6), 062111 (2007).
38. R. B. Saager and A. J. Berger, "Direct characterization and removal of interfering absorption trends in two-layer turbid media," *J. Opt. Soc. Am. A Opt. Image Sci. Vis.* **22**(9), 1874–1882 (2005).
39. F. Fabbri, A. Sassaroli, M. E. Henry, and S. Fantini, "Optical measurements of absorption changes in two-layered diffusive media," *Phys. Med. Biol.* **49**(7), 1183–1201 (2004).
40. G. Strangman, M. A. Franceschini, and D. A. Boas, "Factors affecting the accuracy of near-infrared spectroscopy concentration calculations for focal changes in oxygenation parameters," *Neuroimage* **18**(4), 865–879 (2003).